Please cite the Published Version

Elsayed, Rasha H. , Mahmoud, Ayman M , El-Toumy, Sayed A. , Ahmed, Sayed A. , Salah, Bashir , Lamsabhi, Al Mokhtar and Kamel, Emadeldin M (2025) Unveiling the Molecular Mechanisms of Squalene Epoxidase Inhibition by Flavonoids from Erythrina speciosa: Integrative Computational and Experimental Insights. Revista Brasileira De Farmacognosia, 35. pp. 599-618.

DOI: https://doi.org/10.1007/s43450-025-00649-5

Publisher: Springer

Version: Accepted Version

Downloaded from: https://e-space.mmu.ac.uk/642144/

Usage rights: Creative Commons: Attribution 4.0

Additional Information: This is an author accepted manuscript of an article published in Revista Brasileira De Farmacognosia, by Springer. This version is deposited with a Creative Commons Attribution 4.0 licence [https://creativecommons.org/licenses/by/4.0/], in accordance with Man Met's Research Publications Policy. The version of record can be found on the publisher's website.

Data Access Statement: All experimental data and analyses of the study are included in this manuscript.

Enquiries:

If you have questions about this document, contact openresearch@mmu.ac.uk. Please include the URL of the record in e-space. If you believe that your, or a third party's rights have been compromised through this document please see our Take Down policy (available from https://www.mmu.ac.uk/library/using-the-library/policies-and-guidelines)

- 1 Unveiling the Molecular Mechanisms of Squalene Epoxidase
- 2 Inhibition by Flavonoids from Erythrina speciosa: Integrative
- **3 Computational and Experimental Insights**
- 4 Rasha H. Elsayed^{a, 0000-0003-3284-4227}, Ayman M. Mahmoud^{b,c, 0000-0003-0279-6500}, Sayed A. El-
- $5 \quad Toumy^{d,\ 0000-0002-4699-1562},\ Sayed\ A.\ Ahmed^{a,e,\ 0000-0001-5384-2621},\ Bashir\ Salah^{f,\ 0000-0003-2709-1600},\ Sayed\ A.\ Ahmed^{a,e,\ 0000-0001-5384-2621},\ Bashir\ Sayed\ Ahmed^{a,e,\ 0000-0001-5384-2621},\ Bashir\ Sayed\ Ahmed^{a,e,\ 0000-0001-5384-2621},\ Bashir\ Sayed\ Ahme$
- 6 ^{760X}, Al Mokhtar Lamsabhi^{g,h*}, 0000-0002-1509-2513, Emadeldin M. Kamel^{a*}, 0000-0002-1279-9564
- 7 ^a Chemistry Department, Faculty of Science, Beni-Suef University, Beni-Suef 62514,
- 8 Egypt
- 9 b Department of Life Sciences, Faculty of Science and Engineering, Manchester
- 10 Metropolitan University, Manchester M1 5GD, UK
- 11 ° Molecular Physiology Division, Zoology Department, Faculty of Science, Beni-Suef
- 12 University, Beni-Suef 62514, Egypt
- d Department of Chemistry of Tannins, National Research Centre, Dokki, Cairo, 12622
- 14 Egypt
- ^d Faculty of Engineering, Nahda University, Beni-Suef, Egypt
- 16 f Department of Industrial Engineering, College of Engineering, King Saud University,
- 17 P.O. Box 800, Riyadh 11421, Saudi Arabia.
- 18 g Departamento de Química, Módulo 13, Universidad Autónoma de Madrid, Campus de
- 19 Excelencia, Cantoblanco, 28049 Madrid, Spain
- 20 h Institute for Advanced Research in Chemical Sciences, Universidad Autónoma de
- 21 Madrid, 28049 Madrid, Spain
- 22 *Corresponding author:
- 23 **Emadeldin M. Kamel**
- 24 Chemistry Department, Faculty of Science, Beni-Suef University, Beni-Suef 62514,
- 25 Egypt; emad.abdelhameed@science.bsu.edu.eg

Abstract

26

27

28

29

30

31

32

33

34

35

36

37

38

39

40

41

42

43

44

45

46

47

Squalene epoxidase is a key enzyme in the cholesterol biosynthesis pathway, making it a promising therapeutic target for cholesterol-related disorders. In this study, we integrated computational and experimental approaches to investigate the inhibitory potential of flavonoids isolated from Erythrina speciosa Andrews, Fabaceae, against squalene epoxidase. Molecular docking revealed strong binding affinities for apigenin and vitexin, driven by hydrophobic and electrostatic interactions with critical residues in the squalene epoxidase active site. Molecular dynamics simulations confirmed their binding stability, with low root mean square deviation values, consistent hydrogen bonding, and distinct conformational states supported by potential energy landscape analysis. Interaction energies calculations and binding free energy calculations using MM/PBSA highlighted their favorable binding free energies, underscoring their high affinity for squalene epoxidase. Absorption, distribution, metabolism, and excretion-toxicity analysis demonstrated that both apigenin and vitexin possess favorable drug-like properties, including high bioavailability and compliance with Lipinski's rule of five. Experimental validation through in vitro assays confirmed these findings, with apigenin and vitexin exhibiting low IC₅₀ values (4.70 \pm 0.09 and 3.13 \pm 0.23 μ M, respectively). Enzyme kinetics revealed distinct inhibition mechanisms: apigenin as a mixed inhibitor (Ki = 2.32 μ M) and vitexin as a noncompetitive inhibitor (Ki = 3.18 μ M). This study highlights apigenin and vitexin as potent squalene epoxidase inhibitors, presenting them as promising lead compounds for further pharmacological development. Moreover, the alignment between computational predictions and experimental results underscores the

- 48 reliability of the employed computational pipeline, paving the way for future structure-
- 49 based drug design targeting squalene epoxidase and related enzymes.

Keywords

50

53

54

55

56

57

58

59

60

61

62

63

64

65

66

67

68

69

70

- 51 Enzyme inhibition mechanism; Cholesterol-lowering therapeutics; Enzyme kinetics;
- 52 Natural product inhibitors; Molecular modeling

1. Introduction

Squalene epoxidase is a key enzyme in the cholesterol synthesis pathway, responsible for catalyzing the initial oxygenation of squalene into 2,3-oxidosqualene. (Zhang et al. 2024). This reaction represents a critical regulatory node, as it commits squalene towards sterol production, including cholesterol in humans and ergosterol in fungi (Chua et al. 2020). Dysregulation of squalene epoxidase activity is associated with various pathophysiological conditions, such as hypercholesterolemia, metabolic syndrome, and hormone-dependent cancers like breast and prostate cancer (Giacomini et al. 2021). Furthermore, overexpression of squalene epoxidase has been linked to poor prognosis in certain cancers, making it a potential biomarker for tumor progression (Cirmena et al. 2018). In addition to its relevance in human diseases, squalene epoxidase serves as a promising target for antifungal agents, as the inhibition of ergosterol synthesis in fungi compromises cell membrane integrity, leading to cell death. Existing squalene epoxidase inhibitors, such as terbinafine, have demonstrated clinical success, particularly in treating fungal infections, but challenges such as resistance and off-target effects highlight the need for novel, selective inhibitors (Cirmena et al. 2018). Therefore, a deeper understanding of the enzyme's structural dynamics, substrate interactions, and inhibition mechanisms is crucial for the rational design of next-generation therapeutics.

Erythrina speciosa Andrews, a member of the Fabaceae family, is a tropical plant widely recognized for its ornamental value and traditional medicinal uses (Fahmy et al. 2020a). Native to South America, this species has been extensively studied for its diverse chemical constituents, which include alkaloids, flavonoids, terpenoids, and phenolic acids (Konozy et al. 2003; Rambo et al. 2019; Fahmy et al. 2020b). Among these, flavonoids stand out as bioactive secondary metabolites with a wide range of pharmacological activities, such as antioxidant, anti-inflammatory, antitumor, and antimicrobial effects (Hernández-Rodríguez et al. 2019; Alwaili et al. 2024a; Alruhaimi et al. 2024a). The therapeutic potential of flavonoids has been attributed to their ability to modulate biological pathways, interact with enzymes, and scavenge free radicals (Kamel et al. 2016; Kamel et al. 2023a; Alwaili et al. 2024b). Erythrina speciosa, in particular, has shown promising biological activities, including cytotoxic and antidiabetic properties, due to its rich phytochemical profile (Tripathi et al. 2021; Kamel et al. 2025b). In recent years, natural compounds like flavonoids have garnered significant attention as enzyme inhibitors in drug discovery and development (Alruhaimi et al. 2024b; Kamel et al. 2025a). These compounds often exhibit high specificity, lower toxicity, and reduced side effects compared to synthetic counterparts, making them attractive candidates for therapeutic applications (Correia-da-Silva et al. 2014). Their structural diversity allows them to target enzymes involved in various metabolic and signaling pathways, including those relevant to cholesterol biosynthesis, inflammation, and oxidative stress (Farzaei et al. 2019). The combined use of in vitro and in silico techniques has revolutionized the study of natural compounds as potential enzyme inhibitors, providing complementary insights into

71

72

73

74

75

76

77

78

79

80

81

82

83

84

85

86

87

88

89

90

91

92

their inhibitory mechanisms and therapeutic potential (Kamel et al. 2024c; Kamel et al. 2024d). In vitro studies offer direct evidence of inhibitory activity by measuring enzyme kinetics and determining critical parameters such as IC₅₀ and Ki values (Kamel et al. 2024b; Alghtani et al. 2024; Kamel et al. 2024a). These experiments are essential for validating the efficacy of natural compounds and their specific interactions with enzymes like squalene epoxidase. On the other hand, in silico methods, including molecular docking, molecular dynamics (MD) simulations, MM/PBSA (Molecular Mechanics Poisson-Boltzmann Surface Area) free energy calculations, and principal component analysis (PCA), offer a deeper understanding of the structural and energetic aspects of enzyme-ligand interactions (Kamel et al. 2024e; Kamel et al. 2022). Docking studies provide initial insights into binding modes and affinities, while MD simulations demonstrate the complex's dynamic behavior throughout time. MM/PBSA calculations are instrumental in quantifying binding free energies, and PCA highlights conformational changes in the enzyme upon ligand binding (Kamel et al. 2024f; Kamel et al. 2023b, c). Additionally, ADMET (Absorption, Distribution, Metabolism, Excretion, and Toxicity) predictions evaluate the pharmacokinetic and safety profiles of the compounds, ensuring their drug-likeness (Norinder and Bergström 2006). Together, these integrated approaches allow for the comprehensive assessment of natural compounds' inhibitory activity against squalene epoxidase, bridging the gap between computational predictions and experimental validation while accelerating the discovery of novel inhibitors. This investigation aims to investigate the inhibitory potential of flavonoids that have been isolated from Erythrina speciosa against squalene epoxidase, a key enzyme in the sterol biosynthesis pathway and a promising target for therapeutic intervention in

94

95

96

97

98

99

100

101

102

103

104

105

106

107

108

109

110

111

112

113

114

115

hypercholesterolemia and fungal infections. By employing a combined *in vitro* and *in silico* approach, this study seeks to elucidate the structural and energetic basis of the interactions between the flavonoids and squalene epoxidase. The *in vitro* analysis will determine the inhibitory potency and mode of action, while *in silico* studies, including molecular docking, MD simulations, MM/PBSA binding energy calculations, potential energy landscape (PEL), and ADMET predictions, will provide a comprehensive understanding of binding affinities, dynamic stability, and pharmacokinetic profiles. This integrative approach aims to identify promising lead compounds from *Erythrina speciosa* flavonoids, laying the foundation for the development of novel squalene epoxidase inhibitors with potential therapeutic applications.

2. Materials and methods

2.1. Phytochemical investigation

2.1.1. General experimental procedure

Commercial-grade solvents were used for the phytochemical investigation. TLC analyses were operated on silica gel 60 GF₂₅₄ plates (Merck) and the compounds were visualized by spraying with NH₃/AlCl₃. Silica gel 60 (Merck) was utilized for column chromatography and the preparative paper chromatography was also used for the separation. The NMR spectra were recorded on Bruker AV-400 spectrometer (400 and 100 MHz for 1 H and 13 C, respectively) using DMSO deuterated solvent for all analyses. The chemical shifts (δ) were reported in parts per million (ppm) from the internal standard tetramethylsilane. The fresh leaves of *Erythrina speciosa* Andrew, Fabaceae, were collected from El-Orman Botanical Garden, Giza, Egypt in June 2021. The plant was authenticated by the Botanists in the garden and the Botanists in the Faculty of

- 140 Science, Beni-Suef University. A voucher specimen (BU-NPL-116-150621) was
- deposited at the Herbarium of our natural products laboratory at the Faculty of Science,
- 142 Beni-Suef University, Egypt.

143

2.1.2. Extraction and isolation

- 144 The shade-dried leaves of Erythrina speciosa (1 kg) were ground and extracted by 145 maceration in 70% methanol (7 l, repeated 4 times) at room temperature. The extract was 146 collected and evaporated under reduced pressure at 50 °C until dry, yielding a black sticky mass (182 g). The crude extract was dissolved in water and then partitioned with 147 148 chloroform (1.5 l, five times) and n-butanol (1.5 l, 5 times). The extracts were collected and evaporated in vacuo to produce chloroform extract (12 g), n-butanol extract (39 g), 149 150 and water extract (109 g). A 25 g portion of the *n*-butanol fraction was chromatographed 151 over a polyamide column (250 g of polyamide), with the column gradient eluted using 152 water and ethanol (100:0 to 0:100). The fractions obtained from the polyamide column 153 were collected and analyzed using paper chromatography, resulting in nine fractions (1-154 9). Fraction 2 was further chromatographed on preparative paper chromatography to yield 155 three subfractions (A, B, and C). Subfraction A was purified on a Sephadex LH-20 156 column, resulting in compound 4 (16 mg). Fraction 5 (3 g) was subjected to silica gel 157 column chromatography, yielding two pure compounds: compound 2 (18 mg) and 3 (23 mg). Fraction 6 (0.94 g) was purified on a silica gel column to obtain compound 1 (19 158 159 mg).
- 160 Apigenin (1): yellow crystals, ¹H NMR (400 MHz, DMSO- d_6) δ 7.90 (2H, d, J = 8.5, H-
- 161 2'/6'), 6.90 (2H, d, J = 8.5, H-3'/5'), 6.70(1H, s, H-3), 6.40 (1H, d, J = 2 Hz, H-8), 6.20
- 162 (1H, d, J = 2 Hz, H-6). ¹³C NMR (100 MHz, DMSO- d_6) δ 181.50 (C-4), 163.80 (C-2),

- 163 163.60 (C-7), 161.40 (C-4'), 161.30 (C-5), 157.20 (C-9), 128.30 (C-2'/6'), 121.10 (C-1'),
- 164 116.80 (C-5'), 115.80 (C-3'), 103.60 (C-10), 102.80 (C-3), 98.70 (C-6), 93.90 (C-8).
- 165 Vitexin (apigenin-8-C-β-glucopyranoside) (2): yellow powder, ¹H NMR (400 MHz,
- 166 DMSO- d_6) δ 13.16 (s, 1H), 8.03 (d, J = 8.3 Hz, 2H), 6.91 (d, J = 8.3 Hz, 2H), 6.77 (s,
- 167 1H), 6.27 (s, 1H), 4.71 (d, J = 9.8 Hz, 1H), 3.86 (d, J = 9.2 Hz, 1H), 3.77 (d, J = 11.6 Hz,
- 168 1H), 3.50 (m, 1H), 3.27 (s, 2H). ¹³C NMR (100 MHz, DMSO-d₆) δ 182.51, 164.41,
- 169 163.39, 161.63, 160.87, 156.46, 129.41, 122.06, 116.32, 105.13, 104.95, 102.89, 98.69,
- 170 82.25, 79.12, 73.88, 71.34, 71.04, 61.76.
- 171 Isovitexin (apigenin-6-C-β-glucopyranoside) (3): yellow powder, ¹H NMR (400 MHz,
- 172 DMSO- d_6) δ 13.57 (s, 1H), 7.93 (d, J = 8.8 Hz, 2H), 6.94 (d, J = 8.8 Hz, 2H), 6.78 (s,
- 173 1H), 6.53 (s, 1H), 4.61 (d, J = 9.8 Hz, 1H), 4.06 (t, J = 9.1 Hz, 1H), 3.70 (dd, J = 11.9,
- 174 1.8 Hz, 1H), 3.43 (dd, J = 11.8, 5.7 Hz, 1H), 3.25 3.10 (m, 2H). ¹³C NMR (100 MHz,
- 175 DMSO-*d*₆) δ 182.41, 163.99, 163.90, 161.67, 161.13, 156.72, 128.93, 121.56, 116.47,
- 176 109.35, 103.83, 103.24, 94.13, 82.02, 79.42, 73.54, 71.08, 70.69, 61.95.
- 177 Neoschaftoside (apigenin-6-C-β-D-glucopyranoside-8-C-β-L-arabinopyranoside) (4):
- 178 yellow powder, ¹H NMR (400 MHz, DMSO- d_6) δ 13.90 (s, 1H), 8.02 (d, J = 8.5 Hz, 2H),
- 179 6.92 (d, J = 8.5 Hz, 2H), 6.78 (s, 1H), 5.48 (br s, 1H), 4.74 (d, J = 9.8 Hz, 1H), 4.09 (s,
- 180 1H) 3.86 3.76 (m, 2H), 3.70 (m, 1H), 3.66 (s, 2H), 3.61 3.52 (m, 1H), 3.44-3.33 (m,
- 181 2H), 3.25 (d, J = 9.0 Hz, 1H), 3.17 (s, 1H). ¹³C NMR (100 MHz, DMSO- d_6) δ 182.66,
- 182 164.55, 162.79, 161.82, 155.50, 129.43, 121.90, 116.37, 110.86, 103.88, 103.67, 102.73,
- 183 82.33, 79.14, 73.70, 71.30, 71.12, 71.05, 70.39, 70.23, 67.08, 63.68, 61.84.

2.2. In silico studies

184

185

186

187

188

189

190

191

192

193

194

195

196

197

198

199

200

201

202

203

204

205

2.2.1. System preparation

To guarantee stability, the flavonoid structures utilized in this investigation underwent geometry optimization. Using the 6-311G(d,p) basis set, this procedure was carried out at the B3LYP functional level, establishing each structure as a real energy minimum by demonstrating the absence of imaginary frequencies (Lee et al. 1988; Becke 1988; Hehre et al. 1986). The three-dimensional structure of human squalene epoxidase was retrieved from the Protein Data Bank (PDB ID: 6C6N, resolution 2.30 Å) and subjected to modeling to restore missing residues using Swiss-PdbViewer (Guex and Peitsch 1997). Structural refinement of the squalene epoxidase model included an initial inspection with UCSF Chimera, which involved removing nonstandard residues to prepare the enzyme for further analysis (Pettersen et al. 2004). For molecular docking, AutoDock Tools 1.5.6 (ADT) was employed to define a grid box around the enzyme's active site, and any cocrystallized ligands were removed from the structure (Trott and Olson 2010). The grid box has the following dimensions: size x = 30, size y = 46, and size z = 36; center x = -618.424, center_y = 76.086, and center_z = 55.299. To optimize compatibility with docking, Density Functional Theory computations were performed on isolated flavonoids using Gaussian 16, ensuring their geometries were refined for accurate interaction studies (Frisch et al. 2016). The final preparation steps involved assigning Gasteiger charges to isolated phytochemicals and Kollman charges to the squalene epoxidase enzyme, completing the setup for the molecular docking experiments.

2.2.2. Molecular docking analysis

The preparation of the squalene epoxidase structure for docking involved a series of refinements using AutoDock Tools (ADT). To improve possible hydrogen bonding interactions—a crucial component of precise docking simulations—polar hydrogen atoms were incorporated into the enzyme model. Grid box parameters were meticulously defined to encompass the active site residues entirely, ensuring precise targeting of the binding region (Kamel et al. 2024c). Following these modifications, docking simulations were performed using AutoDock Vina 1.5.6 to evaluate the binding energies of isolated flavonoids within the enzyme's active site (Trott and Olson 2010). The process adhered to a rigorously developed and previously validated protocol established in our laboratory. This protocol emphasized precise grid dimension adjustments to maximize docking accuracy and ensure reliable and reproducible assessments of binding interactions (Alruhaimi et al. 2024b; Kamel et al. 2024d; Kamel et al. 2024e).

Docking Validation Method

The co-crystallized ligand was extracted from the receptor and re-docked under identical conditions. The accuracy of the docking protocol was assessed by calculating the root-mean-square deviation between the top-ranked pose and the original crystallographic coordinates, with an RMSD of less than 2.0 Å indicating an acceptable redocking. Once the method was validated, the clinically relevant antifungal agent terbinafine was docked into the active site of squalene epoxidase using the same parameters. The resulting poses were then evaluated for predicted binding affinity, key ligand-receptor interactions, and congruence with previously reported structure-activity relationships, thereby ensuring the robustness of the docking procedure (the results of docking validation are included in the Supplementary information).

2.2.3. Molecular dynamics simulation

229

230

231

232

233

234

235

236

237

238

239

240

241

242

243

244

245

246

247

248

249

250

251

To investigate the interaction dynamics between squalene epoxidase (PDB ID: 6C6N) and the isolated flavonoids, docking was initially employed to explore the enzymeinhibitor complexes with the most favorable binding energies. For a thorough assessment of their behavior, these high-performing complexes were put through MD simulations using GROMACS 2022.4 that ran for 200 nanoseconds (ns) (Bauer et al. 2022; Abraham et al. 2015). Before initiating the simulations, the docked inhibitors were extracted and prepared for parameterization using GROMACS tools. Interaction parameters were defined using the CHARMM36m force field, and a realistic aquatic environment was simulated using the CHARMM-modified TIP3P water model (Bauer et al. 2022; Abraham et al. 2015). Each inhibitor's geometric parameters and topologies were created using the CGenFF server (https://cgenff.com/) and added to the squalene epoxidase system's full topology file. TIP3P water molecules were used to solvate the enzyme-inhibitor complexes and an unbound squalene epoxidase control, which were placed inside a dodecahedral simulation box. The ultimate simulation box volume, which was around 856.14 nm³, permitted unhindered molecule mobility. To balance the system's charge, a chloride ion was added (MacKerell et al. 1998). Using the steepest descent approach for 10 ps, energy reduction was carried out to guarantee structural integrity by eliminating any steric conflicts or unfavorable atomic interactions (Hess et al. 2008). Two phases of system equilibration ensued, each lasting 100 ps at 300 K: an NVT ensemble phase to stabilize temperature and volume, and an NPT ensemble phase to equilibrate pressure (Parrinello and Rahman 1981). Subsequently, a 200 ns production run was performed under constant temperature 252 (300 K) and pressure (1 bar), enabling a detailed analysis of the stability and molecular

interactions of each enzyme-inhibitor complex throughout the simulation.

2.2.4. Potential energy landscape (PEL)

254

255

256

257

258

259

260

261

262

263

- The PEL of the free enzyme and different flavonoids-squalene epoxidase complexes were constructed using PCA on the MD simulation data to uncover dominant conformational changes. Initially, all frames from the MD trajectory were aligned to remove translational and rotational motions, ensuring the analysis focused solely on internal structural fluctuations. In order to identify the main forms of conformational variation, the analysis focused on backbone atom motions and eliminated non-enzyme atoms. To determine the primary directions of structural dynamics, the eigenvalues and eigenvectors of a covariance matrix of atomic locations were calculated. For additional examination, the first two principal components (PC1 and PC2)—which caused the biggest conformational shifts—were chosen.
- A two-dimensional depiction of the enzyme's conformational space was created by projecting each frame of the MD simulation onto the PC1 and PC2 eigenvectors in order to map the PEL. A grid-based method was used to partition the 2D space into discrete bins, and the probability distribution of frames within each bin was calculated. The Boltzmann equation was used to determine each bin's Gibbs free energy:
- 270 $F = -k_BT \ln(P)$
- where F is the free energy, k_B is the Boltzmann constant, T is the temperature, and P is the probability associated with each bin. Stable conformations were found in regions with

lower free energy, whereas less advantageous forms were found in regions with higher energy.

The free energy data was visualized through a two-dimensional contour map, revealing key energy minima and transition pathways between conformational states. Additionally, a three-dimensional plot was generated to provide a detailed view of the free energy distribution, illustrating the dynamic stability and adaptability of the enzyme. This combined approach offered comprehensive insights into the conformational basins and the transitions governing the enzyme's structural behavior over the course of the simulation.

2.2.5. MM/PBSA analysis

The gmx_MMPBSA tool was used to apply the MM/PBSA approach to the final 50 ns of the MD simulation in order to determine the binding free energy between the squalene epoxidase enzyme and each inhibitor (Valdés-Tresanco et al. 2021). In order to provide a varied and representative group of frames for binding energy estimates, the MD trajectory was preprocessed to obtain snapshots that were uniformly spaced out before the analysis began. When used with GROMACS, the gmx_MMPBSA tool made managing the MD data easier and used the Surface Area and Poisson-Boltzmann approaches to take solvation effects into consideration. Van der Waals interactions, electrostatic forces, polar solvation energy, and non-polar solvation energy were the four main components that were separated out of the binding free energy. The approach yielded precise and reliable estimations of the interaction energy by averaging these values over the trajectory's equilibrated section. To determine the relative contributions of various interaction types to the total binding strength, each energy term was examined separately.

2.2.6. Absorption, distribution, metabolism, excretion, and toxicity analysis

The pharmacokinetic properties of the tested compounds, including their absorption, distribution, metabolism, excretion, and toxicity (ADMET), were evaluated using SwissADME (http://www.swissadme.ch/) to predict their s druglikeness properties (Daina et al. 2017). The SwissADME platform carried out a thorough analysis, assessing important aspects like blood-brain barrier penetration, gastrointestinal absorption, and the compounds' drug-likeness using accepted standards like Veber's guidelines, Ghose's rules, and Lipinski's rule of five. The platform evaluated the possibility of interactions with cytochrome P450 enzymes in order to forecast metabolic behavior, finding possible locations that would be vulnerable to metabolic changes.

2.3. In vitro inhibitory activity assays

2.3.1. Chemicals and reagents

For the *in vitro* studies, recombinant human squalene epoxidase, a critical enzyme in the investigation, was obtained from MyBioSource (7030346). Chemicals and solvents of the highest commercially available purity, usually HPLC grade, were used to guarantee the correctness of all experimental techniques. According to earlier research, radiolabeled [14C]-squalene was created utilizing tried-and-true procedures to allow for accurate activity monitoring (Philippe et al. 2018). High-quality reagents necessary for the enzymatic tests were provided by Cusabio for the recombinant human NADPH cytochrome P450 reductase and Sigma-Aldrich for the recombinant human superoxide dismutase (SOD). To standardize the experimental conditions, trisnorsqualene

cyclopropylamine was employed as a positive control (10 µM), acting as a constant point of comparison and confirmation during the trials.

2.3.2. Squalene epoxidase inhibitory activity assay

317

318

319

320

321

322

323

324

325

326

327

328

329

330

331

332

333

334

335

336

337

The inhibitory assay was carried out in accordance with published procedures (Abe et al. 2000). 20 mM Tris-HCl at pH 7.4, 1.5 mg/ml recombinant squalene epoxidase, 0.05 U recombinant human NADPH cytochrome P450 reductase, 0.1 mM flavin adenine dinucleotide (FAD), and 0.1% Triton X-100, which served as a stand-in for the supernatant protein factor, were all added to a 200 µl reaction buffer. The addition of 50 μM [14C]-squalene and 1 mM NADPH as substrates started the enzymatic activity. After dissolving the test chemicals in two milliliters of ethanol, they were added to the reaction mixture. The combination was first incubated for 15 minutes at 37 °C, and then it was incubated for another 60 minutes to allow the reaction to finish. 200 µl of 10% potassium hydroxide in methanol and 10 µl of 0.1% cold carrier squalene and oxidosqualene dissolved in ethanol were added to stop the enzyme activity. After that, 0.5 1 of dichloromethane was used for lipid extraction, and a 5% ethyl acetate in hexane solvent solution was used to separate the lipid fraction on preparative thin-layer chromatography (TLC) plates. TLC scanning was used to measure the separated chemicals' radioactivity. To ensure accurate measurement of squalene epoxidase activity in vitro, human recombinant SOD was included in the assay to neutralize any superoxide radicals formed during the reaction.

2.3.3. Enzyme kinetics analysis

This assay involved reevaluating previously tested materials with different substrate and inhibitor doses under carefully monitored experimental conditions. Using four distinct substrate doses (0.125, 0.25, 0.375, and 0.50 mM) and matching inhibitor concentrations chosen based on previous IC₅₀ values, the time-dependent inhibition was evaluated in triplicate. (Abe et al. 2000). Ten micrograms of squalene epoxidase and the selected inhibitor were added to each reaction mixture, which had a total volume of 200 microliters. 20 µl samples were taken from the inhibited squalene epoxidase solution at time intervals of 0, 10, 20, and 30 minutes, and they were promptly moved to 180 µL of reaction buffer. This buffer contained 5 µM [14C], 0.1 mM FAD, 1 mM NADPH, 0.1% Triton X-100, 0.05 U NADPH-cytochrome P450 reductase, and 20 mM Tris-HCl (pH 7.4).-squalene. To guarantee a full reaction, the reaction mixtures were then incubated for an extra 60 minutes at 37 °C. Plotting the reciprocal of substrate concentration (1/[S]) against the reciprocal of reaction velocity (1/V) allowed for the creation of a Lineweaver-Burk plot, which was used to examine the inhibition mechanism. This plot enabled the determination of the inhibition constant (K_i), which provided insights into the type and potency of the inhibition. Both the K_i and IC₅₀ values were derived through nonlinear regression analysis using GraphPad Prism 9.0 software.

3. Results and discussion

338

339

340

341

342

343

344

345

346

347

348

349

350

351

352

353

354

355

356

357

358

359

360

3.1. Phytochemical studies

The phytochemical analysis of the *n*-butanol soluble fraction led to the isolation of four flavonoids. The structures of these isolated compounds were confirmed using 1 H-NMR and 13 C-NMR spectroscopy. The compounds were identified as apigenin (1) (Mariappan et al. 2012), apigenin-8-C- β -glucopyranoside (vitexin) (2) (Kim et al. 2005), apigenin-6-

- C- β -glucopyranoside (isovitexin) (3) (Peng et al. 2005), and apigenin-6-C- β -D-
- 362 glucopyranoside-8-*C*-β-L-arabinopyranoside (neoschaftoside) (**4**) (Xie et al. 2003).

3.2. Molecular docking analysis

365

366

367

368

369

370

371

372

373

374

375

376

377

378

379

380

381

382

383

384

385

386

387

The docking analysis of the four flavonoids isolated from Erythrina speciosa against squalene epoxidase provides significant insights into their binding characteristics, as illustrated in Figures 1 and 2. The binding affinities reveal that apigenin (-9.5 kcal/mol) and vitexin (-9.2 kcal/mol) exhibit the strongest interactions, while isovitexin (-8.2 kcal/mol) and neoschaftoside (-5.9 kcal/mol) show moderate to weaker binding. Figures 1A and 2A depict the positioning of these ligands within squalene epoxidase, where apigenin, isovitexin, and vitexin are deeply embedded in the primary binding pocket. In contrast, neoschaftoside occupies an alternative binding site on the enzyme surface, as shown in Figure 2A. The LigPlot representations (Figures 1C and 2C) detail the critical residues involved in stabilizing the ligand-enzyme complexes. Apigenin forms strong hydrophobic interactions with Leu333, Leu509, and Tyr195, contributing to its high binding affinity. Similarly, vitexin demonstrates robust interactions with Pro389, Asp408, and Leu287, as seen in Figure 2C. Isovitexin interacts with residues such as Leu134, Asp408, and Ala284 (Figure 1C), although its binding within the pocket is less optimal. Neoschaftoside, binding on the enzyme surface, engages in interactions with His522, Ala525, and Tyr529 (Figure 2C), indicating a potential allosteric inhibition mechanism. The surface representations in Figures 1B and 2B further illustrate the spatial arrangement of the ligands within squalene epoxidase. Apigenin, isovitexin, and vitexin are well-suited to the enzyme's binding pocket, maximizing hydrophobic and polar contacts. In contrast, neoschaftoside's location on the surface site suggests a unique mode of action distinct from the other flavonoids. Thus, the docking results (Figures 1 and 2) suggest that apigenin and vitexin are promising lead compounds for squalene epoxidase

inhibition due to their high binding affinities and deep interactions within the primary binding pocket. Neoschaftoside, with its surface binding location, may act through a novel inhibitory mechanism, while isovitexin might require further structural modifications to improve its binding efficiency. These findings underscore the potential of these flavonoids as inhibitors and warrant further experimental validation.

3.3. Molecular dynamics simulation

In this section, we present and discuss the key findings from our MD simulations. Our analysis focuses on a range of parameters that provide insight into structural stability, conformational flexibility, and interaction profiles, including root mean square deviation (RMSD), radius of gyration (Rg), solvent-accessible surface area (SASA), root mean square fluctuation (RMSF), hydrogen bonding patterns, interaction energy profiles, PEL, and binding free energy estimates via MM/PBSA. By integrating these metrics, we gain a comprehensive perspective on the behavior and stability of the simulated system throughout the trajectory.

3.3.1. Molecular stability and dynamic behavior

The RMSD analysis of the four flavonoid-squalene epoxidase complexes provides insights into the stability and structural dynamics during the 200 ns MD simulation, as shown in Figure 3. Figure 3A represents the RMSD of the flavonoids relative to the squalene epoxidase binding site, whereas Figure 3B illustrates the RMSD of the enzyme backbone for both the free enzyme and its complexes with the flavonoids. In Figure 3A, the RMSD values reveal distinct binding stability trends among the flavonoids. Apigenin exhibited the lowest RMSD fluctuations, remaining consistently below 0.5 nm throughout the simulation, indicating its strong and stable binding to the squalene

epoxidase active site. Vitexin also demonstrated low RMSD values, maintaining structural stability similar to apigenin. Isovitexin showed slightly higher fluctuations, with RMSD values reaching around 0.8 nm, reflecting moderate stability in its binding interactions. In contrast, neoschaftoside displayed the highest RMSD fluctuations, with values exceeding 2.5 nm after 50 ns. This suggests significant movement or weaker binding of neoschaftoside, consistent with its occupation of an alternative surface binding site. The RMSD analysis of the enzyme backbone highlights the structural stability of squalene epoxidase in both the free and bound states is represented in Figure 3B. The free enzyme maintained low RMSD values, remaining under 0.2 nm throughout the simulation, indicating inherent structural rigidity. Among the complexes, apigeninsqualene epoxidase and vitexin-squalene epoxidase exhibited similar low RMSD profiles, signifying minimal perturbation of the enzyme's structure upon binding. Isovitexinsqualene epoxidase showed slightly higher RMSD values, suggesting minor conformational changes in the enzyme structure. Neoschaftoside-squalene epoxidase displayed the highest RMSD values among the complexes, with more pronounced fluctuations, further supporting the hypothesis of weaker binding or surface interaction that introduces flexibility to the enzyme structure. Overall, the RMSD analysis indicates that apigenin and vitexin form the most stable complexes with squalene epoxidase, with minimal structural disruption to the enzyme. Isovitexin shows moderate binding stability, while neoschaftoside exhibits significant instability, likely due to its unique binding site on the enzyme surface. These findings align with the docking results and underscore the potential of apigenin and vitexin as strong inhibitors of squalene epoxidase.

411

412

413

414

415

416

417

418

419

420

421

422

423

424

425

426

427

428

429

430

431

432

The RMSD analysis of the flavonoid structures relative to their initial conformations highlights distinct trends in binding stability over the 200 ns MD simulation (Figure S12A). Apigenin exhibited the lowest RMSD fluctuations (below 0.1 nm), indicating exceptional stability and minimal deviation from its starting configuration. This suggests a highly stable interaction with squalene epoxidase, consistent with its deep embedding in the enzyme's active site. Vitexin displayed slightly higher RMSD values, fluctuating but generally remaining below 0.15 nm. This indicates a stable binding conformation, though with occasional minor deviations. Isovitexin exhibited moderate RMSD values (up to 0.2 nm), reflecting slightly less stable binding but maintaining an overall consistent interaction. Conversely, neoschaftoside showed the highest RMSD values, frequently exceeding 0.2 nm. This significant deviation indicates considerable conformational flexibility, consistent with its occupation of an alternative binding site on the enzyme surface and weaker overall binding stability. Hydrogen bonding profiles revealed additional distinctions in the interaction dynamics of the flavonoid-squalene epoxidase complexes (Figure S12B). Vitexin formed the highest and most consistent number of hydrogen bonds, averaging 6-7 bonds throughout the simulation. This robust hydrogen bond network supports its high binding affinity and stable interaction within the squalene epoxidase binding pocket. Isovitexin maintained a moderate hydrogen bond count (4-5 bonds on average), which correlates with its moderately stable binding observed in the RMSD analysis. Neoschaftoside exhibited the weakest hydrogen bonding profile, forming only 1-2 bonds on average, further reinforcing its characterization as a weaker binder with surface-level interactions. Interestingly, apigenin formed fewer hydrogen bonds (2–3 bonds on average) compared

434

435

436

437

438

439

440

441

442

443

444

445

446

447

448

449

450

451

452

453

454

455

to vitexin. Despite this, its binding stability is likely driven by strong hydrophobic interactions with key residues, as previously observed in docking studies. These findings align with docking analysis, highlighting the superior binding stability of apigenin and vitexin. Figure S13A highlights the RMSF values of individual residues for free and ligand-bound squalene epoxidase. The free squalene epoxidase displays the lowest fluctuations, particularly in the active site and secondary structural elements, indicating inherent structural stability. The apigenin-squalene epoxidase and vitexin-squalene epoxidase complexes show similar low fluctuations across the enzyme, especially in residues forming the binding pocket, suggesting strong and stable binding. In contrast, isovitexinsqualene epoxidase displays slightly elevated RMSF values, particularly in flexible loop regions around residues 300–350, indicating moderate perturbations in enzyme stability. Neoschaftoside-squalene epoxidase exhibits the highest fluctuations in residues 300–350 and 450-500, consistent with its surface binding and the lack of strong interactions anchoring it to the enzyme. The Rg profile, depicted in Figure S13B, provides insights into the compactness of squalene epoxidase in its free and bound forms. The free enzyme maintains an Rg of ~2.22 nm throughout the simulation, reflecting its structural integrity. The apigeninsqualene epoxidase and vitexin-squalene epoxidase complexes exhibit slightly increased Rg values (~2.23 nm), indicative of stable and compact conformations due to deep binding within the active site. The isovitexin-squalene epoxidase complex demonstrates higher Rg values (~2.24-2.25 nm) with moderate fluctuations, suggesting minor

conformational changes in the enzyme structure. The neoschaftoside-squalene epoxidase

457

458

459

460

461

462

463

464

465

466

467

468

469

470

471

472

473

474

475

476

477

478

complex exhibits the highest Rg (\sim 2.26–2.27 nm) and increased variability, indicating reduced compactness due to surface-level binding, which introduces greater flexibility to the overall enzyme structure.

The solvent-accessible surface area, shown in Figure S13C, reflects the extent of solvent exposure of the enzyme. The free squalene epoxidase maintains consistent SASA values (~205 nm²), demonstrating stable solvent accessibility. The apigenin-squalene epoxidase and vitexin-squalene epoxidase complexes exhibit reduced SASA (~202–204 nm²), corresponding to their deep embedding in the binding pocket, which shields parts of the enzyme from solvent exposure. The isovitexin-squalene epoxidase complex shows slightly higher SASA values (~206–208 nm²), reflecting partial solvent exposure due to suboptimal binding. Neoschaftoside-squalene epoxidase demonstrates the highest SASA (~210–212 nm²), consistent with its surface binding, which leaves most of the enzyme exposed to the solvent. These findings reinforce the potential of apigenin and vitexin as strong inhibitors of squalene epoxidase, while structural optimization may be required to enhance the inhibitory potential of isovitexin and neoschaftoside.

3.3.2. Interaction energies

The Coul-SR interaction energy (electrostatic short-range interaction) profiles for the flavonoid-squalene epoxidase complexes give information on the strength of electrostatic interactions (Figure S14 A). The optimum (lowest) Coul-SR energy values are displayed by vitexin-squalene epoxidase, which continuously hovers around -250 kJ/mol over the 200 ns simulation, suggesting robust and steady electrostatic interactions inside the binding pocket. Apigenin-squalene epoxidase also shows unfavorable Coul-SR energy values, supporting its hydrophobic binding within the pocket. In contrast, isovitexin-

squalene epoxidase displays moderately favorable electrostatic, while neoschaftoside-squalene epoxidase shows weaker interactions due to its surface-level binding and lower interaction depth with squalene epoxidase.

The LJ-SR interaction energy (van der Waals short-range interaction) profiles highlight the contribution of non-polar interactions to complex stability (Figure S14B). Vitexin and apigenin-squalene epoxidase complexes exhibits the most favorable LJ-SR energy values, underscoring their strong hydrophobic interactions with the squalene epoxidase binding site. The isovitexin-squalene epoxidase complex shows intermediate LJ-SR energy values, while neoschaftoside-squalene epoxidase displays the weakest van der Waals interactions, correlating with its less stable and surface-oriented binding mode. The combined analysis of Coul-SR and LJ-SR interaction energies underscores the superior binding affinities of vitexin and apigenin toward squalene epoxidase, driven by strong electrostatic and van der Waals interactions. These observations align with their deeply embedded and stable binding modes observed in RMSD and hydrogen bonding analyses. In contrast, neoschaftoside's weaker interaction energies and isovitexin's moderate profile highlight the need for structural optimization to enhance their binding efficacy. The results further emphasize the potential of vitexin and apigenin as promising lead compounds for squalene epoxidase inhibition.

3.3.3. Potential energy landscape

The potential energy landscape (PEL) analysis provides valuable insights into the conformational dynamics of free squalene epoxidase and its complexes with flavonoids (Figures 4 and 5). The free squalene epoxidase (Figure 4) exhibits a broad and symmetric energy basin centered around the origin in the 2D contour map, reflecting high

conformational flexibility. This indicates that in its apo form, the enzyme explores a wide range of low-energy conformations, characteristic of an unbound state. The binding of flavonoids introduces varying degrees of conformational restriction, as evident in the PEL profiles. The apigenin/squalene epoxidase complex (Figure 4) demonstrates a significantly narrower energy basin with a deep well in the 3D PEL, suggesting a more stable and confined conformational space. This stabilization likely arises from strong hydrophobic and hydrogen-bonding interactions, as corroborated by structural analysis in Figure 6, which highlights key residues such as E165, F165, and L324. These interactions not only stabilize the enzyme structure but also contribute to apigenin's strong inhibitory potential. In contrast, the isovitexin/squalene epoxidase complex (Figure 4) reveals a broader energy basin with a relatively shallow energy well. This indicates weaker binding and reduced structural stabilization compared to apigenin. The structural visualization in Figure 6 shows that isovitexin interacts with residues such as M381, I334, and H226, but with fewer hydrogen bonds and hydrophobic contacts. This aligns with the less confined PEL and suggests weaker inhibitory potential for isovitexin. Further insights are provided by the neoschaftoside and vitexin complexes (Figure 5). Neoschaftoside exhibits an intermediate PEL profile, with a moderately deep energy well reflecting partial stabilization of squalene epoxidase upon binding. Its interactions with key residues like H522 and E500 involve hydrogen bonding and aromatic stacking, as shown in Figure 6, supporting moderate binding affinity. On the other hand, the vitexin/squalene epoxidase complex demonstrates a highly confined energy landscape with a deep and asymmetric

energy well. The structural data reveal extensive hydrogen bonding with residues such as

526

527

528

529

530

531

532

533

534

535

536

537

538

539

540

541

542

543

544

545

546

547

T417, L416, and M413, alongside strong hydrophobic interactions. This robust interaction network corresponds to vitexin's tight binding and significant stabilization of the enzyme. To sum up, the combined PEL and structural analysis reveal that apigenin and vitexin are the strongest inhibitors of squalene epoxidase, as evidenced by their deep and narrow energy wells and extensive residue interactions.

3.3.4. MM/PBSA analysis

549

550

551

552

553

554

555

556

557

558

559

560

561

562

563

564

565

566

567

568

569

570

571

The MM/PBSA results provide detailed insights into the binding free energy contributions of the flavonoids to squalene epoxidase based on the final 50 ns of MD trajectory (Table 1). The energy components considered include van der Waals energy (ΔE_{vdw}) , electrostatic energy (ΔE_{ele}) , solvation energy (ΔG_{solv}) , gas-phase energy (ΔG_{gas}) , and the total binding free energy (ΔG_{total}), which together help evaluate the stability and strength of the flavonoid-squalene epoxidase interactions. Among the flavonoids, vitexin exhibited the most favorable van der Waals interactions and electrostatic interactions with squalene epoxidase, suggesting that it forms strong hydrophobic and hydrogen-bonding interactions within the squalene epoxidase binding pocket. In contrast, apigenin showed significant but slightly weaker interactions. Isovitexin and neoschaftoside had weaker van der Waals interactions and less favorable electrostatic interactions, indicating that these flavonoids interact less favorably with squalene epoxidase. In terms of solvation energy, all complexes experienced unfavorable contributions due to the desolvation penalty upon binding. However, vitexin exhibited the highest solvation penalty, likely due to its polar substituents, which increase the desolvation cost compared to the other flavonoids. The gas-phase energy, which combines van der Waals and electrostatic interactions, was most favorable for vitexin, followed by apigenin.

When considering the total binding free energy (ΔG_{total}), vitexin exhibited the most favorable binding (-37.39 kcal/mol), indicating strong and stable binding to squalene epoxidase. This result is consistent with the favorable van der Waals and electrostatic interactions observed for vitexin. Apigenin followed with $\Delta G_{total} = -23.43$ kcal/mol, showing moderate binding affinity due to its significant hydrophobic interactions despite its lower electrostatic contributions. Isovitexin and neoschaftoside showed weaker total binding affinities ($\Delta G_{total} = -16.39$ kcal/mol and -12.90 kcal/mol, respectively), in line with the MD simulations, which suggested that isovitexin binds less efficiently and neoschaftoside binds at the enzyme surface in an allosteric manner. Thus, the MM/PBSA results corroborate the molecular docking and MD simulations, with vitexin emerging as the most potent squalene epoxidase inhibitor, followed by apigenin. These two flavonoids exhibit the strongest binding affinities due to their favorable van der Waals and electrostatic interactions.

3.4. ADMET analysis

The ADMET properties of apigenin, isovitexin, neoschaftoside, and vitexin were analyzed to evaluate their drug-likeness and pharmacokinetic profiles (Table 2). Key properties influencing drug behavior, such as molecular weight (MW), hydrogen bonding potential, lipophilicity, solubility, metabolic stability, and bioavailability, were assessed and are summarized below. Apigenin displayed favorable ADMET properties, aligning well with drug-likeness criteria. Its low molecular weight and a single rotatable bond indicate structural simplicity and limited flexibility, which contribute to higher stability and predictability in biological systems. Apigenin met Lipinski's rule of five with zero violations, showing potential for oral bioavailability. It exhibited high gastrointestinal

(GI) absorption and moderate lipophilicity (log Po/w = 2.11), consistent with effective membrane permeability. However, the compound is not blood-brain barrier (BBB) permeable and shows moderate solubility (logS = -3.94), suggesting limited CNS penetration but suitable systemic exposure. Apigenin interacts with multiple cytochrome P450 enzymes, particularly CYP1A2, CYP2D6, and CYP3A4, which may influence its metabolic stability. Its bioavailability score (0.55) indicates promising drug-likeness. Isovitexin demonstrated suboptimal pharmacokinetic properties compared to apigenin, with a higher molecular weight (432.38 g/mol) and increased flexibility due to three rotatable bonds. The compound violated Lipinski's rule due to excessive hydrogen bond donors (7), which could hinder membrane permeability. Its high polarity (TPSA = 181.05 $Å^2$) and low lipophilicity (log Po/w = -0.02) suggest poor membrane permeability, supported by its low GI absorption. Despite these limitations, isovitexin showed moderate solubility (logS = -2.84) and a bioavailability score of 0.55, indicating some potential for further optimization. Unlike apigenin, isovitexin did not interact with any tested cytochrome P450 enzymes, which may reduce its risk of metabolic interactions but might also limit metabolic activation. Neoschaftoside exhibited the least favorable ADMET properties due to its high molecular weight (564.49 g/mol) and significant polarity (TPSA = 250.97 Å²), which severely restrict its permeability across biological membranes. The compound had three violations of Lipinski's rule (MW > 500, O > 10, OH > 5), emphasizing its limited drug-likeness. Neoschaftoside showed very low bioavailability (0.17), low GI absorption, and poor solubility (logS = -1.99), making it unsuitable for systemic therapeutic applications without structural modifications. Its low lipophilicity (Log Po/w = -1.87) and non-

595

596

597

598

599

600

601

602

603

604

605

606

607

608

609

610

611

612

613

614

615

616

interaction with cytochrome P450 enzymes further underscore its poor pharmacokinetic profile.

Vitexin shared several ADMET properties with isovitexin, including the same molecular weight (432.38 g/mol) and polarity (TPSA = 181.05 Ų), resulting in similar pharmacokinetic challenges. The compound also violated Lipinski's rule due to excessive hydrogen bond donors (7) and exhibited low GI absorption. However, it maintained a moderate solubility profile (logS = -2.84) and bioavailability score (0.55), suggesting potential for oral administration after optimization. Like isovitexin, vitexin did not interact with cytochrome P450 enzymes, highlighting its likely metabolic stability but limited activation potential. Thus, apigenin emerged as the most promising candidate based on its favorable ADMET profile, including high GI absorption, adequate solubility, and good bioavailability. In contrast, isovitexin and vitexin demonstrated limited permeability and absorption, likely due to high polarity and hydrogen bonding, while neoschaftoside displayed poor drug-likeness properties overall.

3.5. In vitro squalene epoxidase inhibitory activity assay

The *in vitro* inhibitory activity and enzyme kinetics analysis of the isolated flavonoids against squalene epoxidase provided crucial insights into their potential as inhibitors. The results are presented in Figure 7, showcasing the dose-response curves, IC₅₀ values, and enzyme kinetic analyses. These findings complement the *in silico* predictions and validate their relevance in identifying effective inhibitors for squalene epoxidase. The dose-response curves (Figure 7A) demonstrated a concentration-dependent inhibition of squalene epoxidase activity by all tested flavonoids. Among the compounds, vitexin and apigenin exhibited the most potent inhibitory activities, with IC₅₀ values of 3.13 ± 0.23

 μM and 4.70 \pm 0.09 μM , respectively (Figure 7B). These values are comparable to the reference inhibitor trisnorsqualene cyclopropylamine (IC₅₀ = $2.76 \pm 0.05 \mu M$), underscoring their efficacy. Conversely, isovitexin and neoschaftoside showed weaker inhibition, with IC₅₀ values of 19.44 \pm 3.84 μ M and 36.24 \pm 2.98 μ M, respectively, aligning with their less favorable binding affinities and interaction profiles observed in the in silico docking and MD simulation studies. The high potency of apigenin and vitexin correlates well with their strong hydrophobic and electrostatic interactions with the squalene epoxidase active site, as identified in MD simulations. Further kinetic characterization was conducted for apigenin and vitexin, the two compounds with the lowest IC₅₀ values. Lineweaver-Burk plots (Figures 7C and 7D) and Michaelis-Menten plots (Figures 7E and 7F) revealed distinct inhibition mechanisms for these flavonoids. Apigenin exhibited a mixed inhibition mode with a K_i value of 2.32 μ M, indicating that it interacts with both the squalene epoxidase active site and an allosteric site, affecting enzyme activity regardless of substrate binding. This is consistent with its predicted binding mode from in silico studies, which highlighted its strong interactions with key catalytic residues. The $K_{\rm m}$ and $V_{\rm max}$ values of apigenin are 10.62 μM and 53.26 μM/min/mg, respectively. In contrast, vitexin demonstrated a noncompetitive inhibition mechanism with a Ki value of 3.18 µM. This suggests that vitexin binds to an allosteric site, inducing conformational changes that impair enzymatic activity without directly obstructing substrate binding. This inhibition mode aligns with its unique binding profile observed in molecular docking, which indicated favorable interactions outside the active site region. The $K_{\rm m}$ and $V_{\rm max}$ values of vitexin are 15.08 μ M and 55.48 μ M/min/mg, respectively.

641

642

643

644

645

646

647

648

649

650

651

652

653

654

655

656

657

658

659

660

661

662

The experimental findings strongly validate the *in silico* predictions. Both apigenin and vitexin, identified as the most potent inhibitors through computational studies, demonstrated superior activity *in vitro*, reflected in their low IC₅₀ values and distinct kinetic behaviors. The weaker inhibition by isovitexin and neoschaftoside further supports their lower binding affinities and suboptimal pharmacokinetic profiles predicted during *in silico* analyses. These results highlight the robustness of combining *in silico* and *in vitro* approaches to identify potent inhibitors. Apigenin and vitexin emerge as promising lead compounds for further development as squalene epoxidase inhibitors, with their mixed and noncompetitive inhibition mechanisms offering complementary therapeutic potential. The study also underscores the need for structural optimization of less active flavonoids like isovitexin and neoschaftoside to enhance their inhibitory efficacy.

4. Conclusion

This study successfully integrates computational and experimental approaches to uncover the molecular mechanisms underlying the inhibition of squalene epoxidase by naturally derived flavonoids from *Erythrina speciosa*. Molecular docking revealed that apigenin and vitexin exhibited the strongest binding affinity among the tested compounds, driven by favorable hydrophobic and electrostatic interactions. MD simulations further highlighted their strong binding stability with squalene epoxidase, supported by stable dynamic behavior, low RMSD values, and consistent hydrogen bonding patterns. Potential energy landscape analysis underscored distinct energetic favorability for their conformational states, corroborating the role of key residues in their binding. The MM/PBSA free energy and interaction energy calculations affirmed the superior binding

free energies of apigenin and vitexin, driven primarily by hydrophobic and electrostatic interactions. These findings were further corroborated by ADMET analysis, which demonstrated that both compounds possess favorable drug-like properties, including high bioavailability and adherence to Lipinski's rule of five.

Importantly, the *in vitro* assays validated the *in silico* predictions, with apigenin and vitexin displaying potent inhibitory activity against squalene epoxidase, as evidenced by their low IC50 values (4.70 \pm 0.09 μ M and 3.13 \pm 0.23 μ M, respectively). Enzyme kinetics analysis revealed distinct mechanisms of inhibition, with apigenin acting as a mixed inhibitor (Ki = 2.32 μ M) and vitexin exhibiting a noncompetitive mode of inhibition (Ki = 3.18 μ M). These findings highlight the potential of apigenin and vitexin as promising lead compounds for the development of novel squalene epoxidase inhibitors, offering therapeutic potential against cholesterol-related disorders. Furthermore, the alignment between *in silico* and experimental results underscores the robustness of the computational pipeline employed, setting a foundation for future structure-based drug design targeting squalene epoxidase and other enzymes critical to metabolic pathways.

Statements and Declarations

Consent to Participate

705 This research does not contain any studies with human participants performed by any of

706 the authors.

Consent to Publish

708 Free

Authors Contributions

709

710 EMK: conceptualization, methodology, project administration, formal analysis, data curation, molecular docking and dynamics analysis, experimental studies, enzyme assay 711 712 development, validation, visualization, preparation of figures and tables, writing – 713 original draft, writing – review and editing, and supervision; RHE: experimental studies, 714 enzyme assay development, and data interpretation; SAEI-T: experimental studies, 715 enzyme assay development, and data interpretation; SAA: validation, visualization, and 716 preparation of figures and tables; BS: supervision, funding acquisition, critical review of 717 results; AlML: conceptualization, methodology, project administration, formal analysis, 718 funding acquisition, writing – original draft, and supervision

Funding

719

727

729

This work was carried out with the support from the project PID2023-150717NB-I00 from Ministerio de Ciencia, Innovacion y Universidades in Spain and the PRIES-CM project Ref: Y2020/EMT-6290 from the Comunidad Autónoma de Madrid. Lastly, the authors express their gratitude to the Centro de Computación Científica of the UAM (CCC-UAM) for providing the computing time. This study received funding from King Saud University, Saudi Arabia through researchers supporting project number (RSP2025R145)

Competing Interests

728 The authors declare no competing interests.

Availability of data and materials

All experimental data and analyses of the study are included in this manuscript.

Acknowledgment

731

739

743

744

745

746 747

748

749

750

751

752

753

754

755 756

757

- 732 This study received funding from King Saud University, Saudi Arabia through
- researchers supporting project number (RSP2025R145). This work was carried out with
- 734 the support from the project PID2023-150717NB-I00 from Ministerio de Ciencia,
- Innovacion y Universidades in Spain and the PRIES-CM project Ref: Y2020/EMT-6290
- 736 from the Comunidad Autónoma de Madrid. Lastly, the authors express their gratitude to
- 737 the Centro de Computación Científica of the UAM (CCC-UAM) for providing the
- 738 computing time.

References

- Abe I, Seki T, Noguchi H (2000) Potent and selective inhibition of squalene epoxidase by synthetic galloyl esters. Biochem Biophys Res Commun 270:137-140.
- 742 https://doi.org/10.1006/bbrc.2000.2399
 - Abraham MJ, Murtola T, Schulz R, Páll S, Smith JC, Hess B, Lindahl E (2015) GROMACS: High performance molecular simulations through multi-level parallelism from laptops to supercomputers. SoftwareX 1-2:19-25. https://doi.org/10.1016/j.softx.2015.06.001
 - Alqhtani HA, Othman SI, Aba Alkhayl FF, Altoom NG, Lamsabhi AM, Kamel EM (2024) Unraveling the mechanism of carbonic anhydrase IX inhibition by alkaloids from *Ruta chalepensis*: aq synergistic analysis of in vitro and in silico data. Biochem Biophys Res Commun 733:150685, https://doi.org/10.1016/j.bbrc.2024.150685
 - Alruhaimi RS, Mahmoud AM, Alnasser SM, Alotaibi MF, Elbagory I, El-Bassuony AA, Lamsabhi AM, Kamel EM (2024a) Integrating computational modeling and experimental validation to unveil tyrosinase inhibition mechanisms of flavonoids from *Alhagi graecorum*. ACS Omega 9:47167-47179. https://doi.org/10.1021/acsomega.4c07624
 - Alruhaimi RS, Mahmoud AM, Elbagory I, Ahmeda AF, El-Bassuony AA, Lamsabhi AM, Kamel EM (2024b) Unveiling the tyrosinase inhibitory potential of phenolics from *Centaurium spicatum*: bridging *in silico* and *in vitro* perspectives. Bioorg Chem 147:107397. https://doi.org/10.1016/j.bioorg.2024.107397
- Alwaili MA, Aba Alkhayl FF, Rudayni HA, Allam AA, Altoom NG, Lamsabhi AM, Kamel EM (2024a)
 Unraveling molecular mechanisms of β-glucuronidase inhibition by flavonoids from
 Centaurea scoparia: integrated in silico and in vitro insights. New J Chem 48:14236 14252. https://doi.org/10.1039/D4NJ02393E
- Alwaili MA, Alkhayl FFA, Rudayni HA, Allam AA, Lamsabhi AM, Kamel EM (2024b) Mechanistic
 insights into β-glucuronidase inhibition by isoprenylated flavonoids from *Centaurea* scoparia: bridging experimental and computational approaches. J Mol Struct
 1322:140354. https://doi.org/10.1016/j.molstruc.2024.140354
- 766 Bauer P, Hess B, Lindahl E (2022) GROMACS 2022.4 Manual. November 16:2022

- Becke AD (1988) Density-functional exchange-energy approximation with correct asymptotic
 behavior. Phys Rev A 38:3098
- Chua NK, Coates HW, Brown AJ (2020) Squalene monooxygenase: a journey to the heart of cholesterol synthesis. Prog Lipid Res 79:101033.
 https://doi.org/10.1016/j.plipres.2020.101033

- Cirmena G, Franceschelli P, Isnaldi E, Ferrando L, De Mariano M, Ballestrero A, Zoppoli G (2018) Squalene epoxidase as a promising metabolic target in cancer treatment. Cancer Lett 425:13-20. https://doi.org/10.1016/j.canlet.2018.03.034
- Correia-da-Silva M, Sousa E, Pinto MMM (2014) Emerging sulfated flavonoids and other polyphenols as drugs: nature as an inspiration. Med Res Rev 34:223-279. https://doi.org/10.1002/med.21282
- Daina A, Michielin O, Zoete V (2017) SwissADME: a free web tool to evaluate pharmacokinetics, drug-likeness and medicinal chemistry friendliness of small molecules. Sci Rep 7:42717. https://doi.org/10.1038/srep42717
- Fahmy NM, Al-Sayed E, Michel HE, El-Shazly M, Singab ANB (2020a) Gastroprotective effects of *Erythrina speciosa* (Fabaceae) leaves cultivated in Egypt against ethanol-induced gastric ulcer in rats. J Ethnopharmacol 248:112297. https://doi.org/10.1016/j.jep.2019.112297
- Fahmy NM, Al-Sayed E, Moghannem S, Azam F, El-Shazly M, Singab AN (2020b) Breaking down the barriers to a natural antiviral agent: antiviral activity and molecular docking of *Erythrina speciosa* extract, fractions, and the major compound. Chem Biodivers 17:e1900511. https://doi.org/10.1002/cbdv.201900511
- Farzaei MH, Singh AK, Kumar R, Croley CR, Pandey AK, Coy-Barrera E, Kumar Patra J, Das G, Kerry RG, Annunziata G, Tenore GC, Khan H, Micucci M, Budriesi R, Momtaz S, Nabavi SM, Bishayee A (2019) Targeting inflammation by flavonoids: novel therapeutic strategy for metabolic disorders. Int J Mol Sci 20:4957. https://doi.org/10.3390/ijms20194957
- Frisch MJ, Trucks GW, Schlegel HB, Scuseria GE, Robb MA, Cheeseman JR, Scalmani G, Barone V, Petersson GA, Nakatsuji H, Li X, Caricato M, Marenich AV, Bloino J, Janesko BG, Gomperts R, Mennucci B, Hratchian HP, Ortiz JV, Izmaylov AF, Sonnenberg JL, Williams, Ding F, Lipparini F, Egidi F, Goings J, Peng B, Petrone A, Henderson T, Ranasinghe D, Zakrzewski VG, Gao J, Rega N, Zheng G, Liang W, Hada M, Ehara M, Toyota K, Fukuda R, Hasegawa J, Ishida M, Nakajima T, Honda Y, Kitao O, Nakai H, Vreven T, Throssell K, Montgomery Jr. JA, Peralta JE, Ogliaro F, Bearpark MJ, Heyd JJ, Brothers EN, Kudin KN, Staroverov VN, Keith TA, Kobayashi R, Normand J, Raghavachari K, Rendell AP, Burant JC, Iyengar SS, Tomasi J, Cossi M, Millam JM, Klene M, Adamo C, Cammi R, Ochterski JW, Martin RL, Morokuma K, Farkas O, Foresman JB, Fox DJ (2016) Gaussian 16 Rev. C.01. Wallingford, CT
- Giacomini I, Gianfanti F, Desbats MA, Orso G, Berretta M, Prayer-Galetti T, Ragazzi E, Cocetta V (2021) Cholesterol metabolic reprogramming in cancer and its pharmacological modulation as therapeutic strategy. Front Oncol 11:682911. https://doi.org/10.3389/fonc.2021.682911
- Guex N, Peitsch MC (1997) SWISS-MODEL and the Swiss-Pdb Viewer: an environment for comparative protein modeling. Electrophoresis 18:2714-2723. https://doi.org/10.1002/elps.1150181505
- Hehre WJ, Radom L, Schleyer PvR, Pople JA (1986) Ab initio molecular orbital theory. John Wiley and Sons, New York.
- Hernández-Rodríguez P, Baquero LP, Larrota HR (2019) Chapter 14 Flavonoids: potential therapeutic agents by their antioxidant capacity. In: Campos MRS (ed) Bioactive

- 814 Compounds. Woodhead Publishing, pp 265-288. https://doi.org/10.1016/B978-0-12-815 814774-0.00014-1
- Hess B, Kutzner C, Van Der Spoel D, Lindahl E (2008) GROMACS 4: algorithms for highly efficient,
 load-balanced, and scalable molecular simulation. J Chem Theory Comput 4:435-447.
 https://doi.org/10.1021/ct700301g

- Kamel EM, Aba Alkhayl FF, Alqhtani HA, Bin-Jumah M, Lamsabhi AM (2024a) Dynamic interactions and inhibitory mechanisms of *Artemisia annua* terpenoids with carbonic anhydrase IX. Int J Biol Macromol 282:136982. https://doi.org/10.1016/j.ijbiomac.2024.136982
- Kamel EM, Ahmed NA, El-Bassuony AA, Hussein OE, Alrashdi B, Ahmed SA, Lamsabhi AM, Arab HH, Mahmoud AM (2022) Xanthine oxidase inhibitory activity of *Euphorbia peplus* L. phenolics. Comb Chem High Throughput Screen 25:1336-1344. https://doi.org/10.2174/1386207324666210609104456.
- Kamel EM, Alkhayl FFA, Alqhtani HA, Bin-Jumah M, Rudayni HA, Lamsabhi AM (2024b) Bridging in *silico* and *in vitro* perspectives to unravel molecular mechanisms underlying the inhibition of β-glucuronidase by coumarins from *Hibiscus trionum*. Biophys Chem 313:107304. https://doi.org/10.1016/j.bpc.2024.107304
- Kamel EM, Alkhayl FFA, Alqhtani HA, Bin-Jumah M, Rudayni HA, Lamsabhi AM (2024c) Dissecting molecular mechanisms underlying the inhibition of β-glucuronidase by alkaloids from *Hibiscus trionum*: integrating in vitro and *in silico* perspectives. Comput Biol Med 180:108969. https://doi.org/10.1016/j.compbiomed.2024.108969
- Kamel EM, Alqhtani HA, Bin-Jumah M, Rudayni HA, El-Bassuony AA, Mokhtar Lamsabhi A (2024d) Deciphering molecular mechanisms underlying the inhibition of β-glucuronidase by xanthones from Centaurium spicatum. Bioorg Chem 150:107609. https://doi.org/10.1016/j.bioorg.2024.107609
- Kamel EM, Alwaili MA, Rudayni HA, Allam AA, Lamsabhi AM (2024e) Deciphering the molecular mechanisms of reactive metabolite formation in the mechanism-based inactivation of cytochrome p450 1B1 by 8-methoxypsoralen and assessing the driving effect of phe268. Molecules 29:1433. https://doi.org/10.3390/molecules29071433
- Kamel EM, Bin-Ammar A, El-Bassuony AA, Alanazi MM, Altharawi A, Ahmeda AF, Alanazi AS, Lamsabhi AM, Mahmoud AM (2023a) Molecular modeling and DFT studies on the antioxidant activity of *Centaurea scoparia* flavonoids and molecular dynamics simulation of their interaction with β-lactoglobulin. RSC Advances 13:12361-12374. https://doi.org/10.1039/D3RA01661G
- Kamel EM, Mahmoud AM, Ahmed SA, Lamsabhi AM (2016) A phytochemical and computational study on flavonoids isolated from *Trifolium resupinatum* L. and their novel hepatoprotective activity. Food Funct 7:2094-2106. https://doi.org/10.1039/C6FO00194G
- Kamel EM, Maodaa S, Al-Shaebi EM, Lamsabhi AM (2024f) Mechanistic insights into the metabolic pathways of vanillin: unraveling cytochrome P450 interaction mechanisms and implications for food safety. Org Biomol Chem 22:6561-6574. https://doi.org/10.1039/D4OB00973H
- Kamel EM, Othman SI, Aba Alkhayl FF, Rudayni HA, Allam AA, Lamsabhi AM (2025a) Mechanistic insights into alkaloid-based inhibition of squalene epoxidase: a combined in silico and experimental approach for targeting cholesterol biosynthesis. Int J Biol Macromol 302:140609. https://doi.org/10.1016/j.ijbiomac.2025.140609

Kamel EM, Othman SI, Rudayni HA, Allam AA, Lamsabhi AM (2025b) Multi-pronged molecular
 insights into flavonoid-mediated inhibition of squalene epoxidase: a pathway to novel
 therapeutics. RSC Advances 15:3829-3848. https://doi.org/10.1039/D4RA09076D

- Kamel EM, Tawfeek AM, El-Bassuony AA, Lamsabhi AM (2023b) Mechanistic aspects of reactive metabolite formation in clomethiazole catalyzed biotransformation by cytochrome P450 enzymes. Org Biomol Chem 21:7158-7172. https://doi.org/10.1039/D30B01014G
- Kamel EM, Tawfeek AM, El-Bassuony AA, Lamsabhi AM (2023c) Mechanistic insights into chloramphenicol-mediated inactivation of cytochrome P450 enzymes and their active site mutants. New J Chem 47:16429-16443. https://doi.org/10.1039/D3NJ02991C
- Kim JH, Lee BC, Kim JH, Sim GS, Lee DH, Lee KE, Yun YP, Pyo HB (2005) The isolation and antioxidative effects of vitexin from *Acer palmatum*. Arch Pharm Res 28:195-202. https://doi.org/10.1007/BF02977715
- Konozy EHE, Bernardes ES, Rosa C, Faca V, Greene LJ, Ward RJ (2003) Isolation, purification, and physicochemical characterization of a D-galactose-binding lectin from seeds of *Erythrina speciosa*. Arch Biochem Biophys 410:222-229. https://doi.org/10.1016/S0003-9861(02)00695-1
- Lee C, Yang W, Parr RG (1988) Development of the Colle-Salvetti correlation-energy formula into a functional of the electron density. Phys rev B 37:785. https://doi.org/10.1103/PhysRevB.37.785
- MacKerell AD, Jr., Bashford D, Bellott M, Dunbrack RL, Jr., Evanseck JD, Field MJ, Fischer S, Gao J, Guo H, Ha S, Joseph-McCarthy D, Kuchnir L, Kuczera K, Lau FTK, Mattos C, Michnick S, Ngo T, Nguyen DT, Prodhom B, Reiher WE, Roux B, Schlenkrich M, Smith JC, Stote R, Straub J, Watanabe M, Wiórkiewicz-Kuczera J, Yin D, Karplus M (1998) All-atom empirical potential for molecular modeling and dynamics studies of proteins. J Phys Chem B 102:3586-3616. https://doi.org/10.1021/jp973084f
- Mariappan G, Sundaraganesan N, Manoharan S (2012) The spectroscopic properties of anticancer drug apigenin investigated by using DFT calculations, FT-IR, FT-Raman and NMR analysis. Spectrochim Acta A Mol Biomol Spectrosc 95:86-99. https://doi.org/10.1016/j.saa.2012.04.089
- Norinder U, Bergström CAS (2006) Prediction of ADMET Properties. ChemMedChem 1:920-937. https://doi.org/10.1002/cmdc.200600155
- Parrinello M, Rahman A (1981) Polymorphic transitions in single crystals: A new molecular dynamics method. J Appl phys 52:7182-7190. https://doi.org/10.1063/1.328693
- Peng J, Fan G, Hong Z, Chai Y, Wu Y (2005) Preparative separation of isovitexin and isoorientin from *Patrinia villosa* Juss by high-speed counter-current chromatography. J Chromatogr A 1074:111-115. https://doi.org/10.1016/j.chroma.2005.03.067
- Pettersen EF, Goddard TD, Huang CC, Couch GS, Greenblatt DM, Meng EC, Ferrin TE (2004) UCSF Chimera—A visualization system for exploratory research and analysis. J Comput Chem 25:1605-1612. https://doi.org/10.1002/jcc.20084
- Philippe N, Rivron L, De Bruin B, Schofield J, Roy S (2018) Two new convenient syntheses of 14C-squalene from turbinaric acid. J Labelled Comp Radiopharm 61 (12):878-884. https://doi.org/10.1002/jlcr.3672
- Rambo DF, Biegelmeyer R, Toson NSB, Dresch RR, Moreno PRH, Henriques AT (2019) The genus L.: a review on its alkaloids, preclinical, and clinical studies. Phytother Res 33:1258-1276. https://doi.org/10.1002/ptr.6321
- Tripathi SK, Behera S, Panda M, Zengin G, Biswal BK (2021) A comprehensive review on pharmacology and toxicology of bioactive compounds of *Lagerstroemia speciosa*(L.)

907	Pers. Curr Tradit Med 7:504-513.
908	https://doi.org/10.2174/2215083806999201211213931
909	Trott O, Olson AJ (2010) AutoDock Vina: improving the speed and accuracy of docking with a
910	new scoring function, efficient optimization, and multithreading. J Comput Chem
911	31:455-461. https://doi.org/10.1002/jcc.21334
912	Valdés-Tresanco MS, Valdés-Tresanco ME, Valiente PA, Moreno E (2021) gmx_MMPBSA: a new
913	tool to perform end-state free energy calculations with GROMACS. J Chem Theory
914	Comput 17:6281-6291. https://doi.org/10.1021/acs.jctc.1c00645
915 916	Xie C, Veitch NC, Houghton PJ, Simmonds MSJ (2003) Flavone <i>C</i> -glycosides from <i>Viola yedoensis</i> Makino. Chem Pharm Bull 51:1204-1207. https://doi.org/10.1248/cpb.51.1204
910	Zhang L, Cao Z, Hong Y, He H, Chen L, Yu Z, Gao Y (2024) Squalene epoxidase: its regulations and
918	links with cancers. Int J Mol Sci 25:3874. https://doi.org/10.3390/ijms25073874
	mine that salisors into the ost 25.557 interprite denoty in the salisors in th
919	
920	
720	
921	
922	
923	
923	
924	
925	
007	
926	
927	
721	
928	
929	
000	
930	
931	
701	
932	
933	
024	
934	
935	
,50	
936	

937 Figure legends

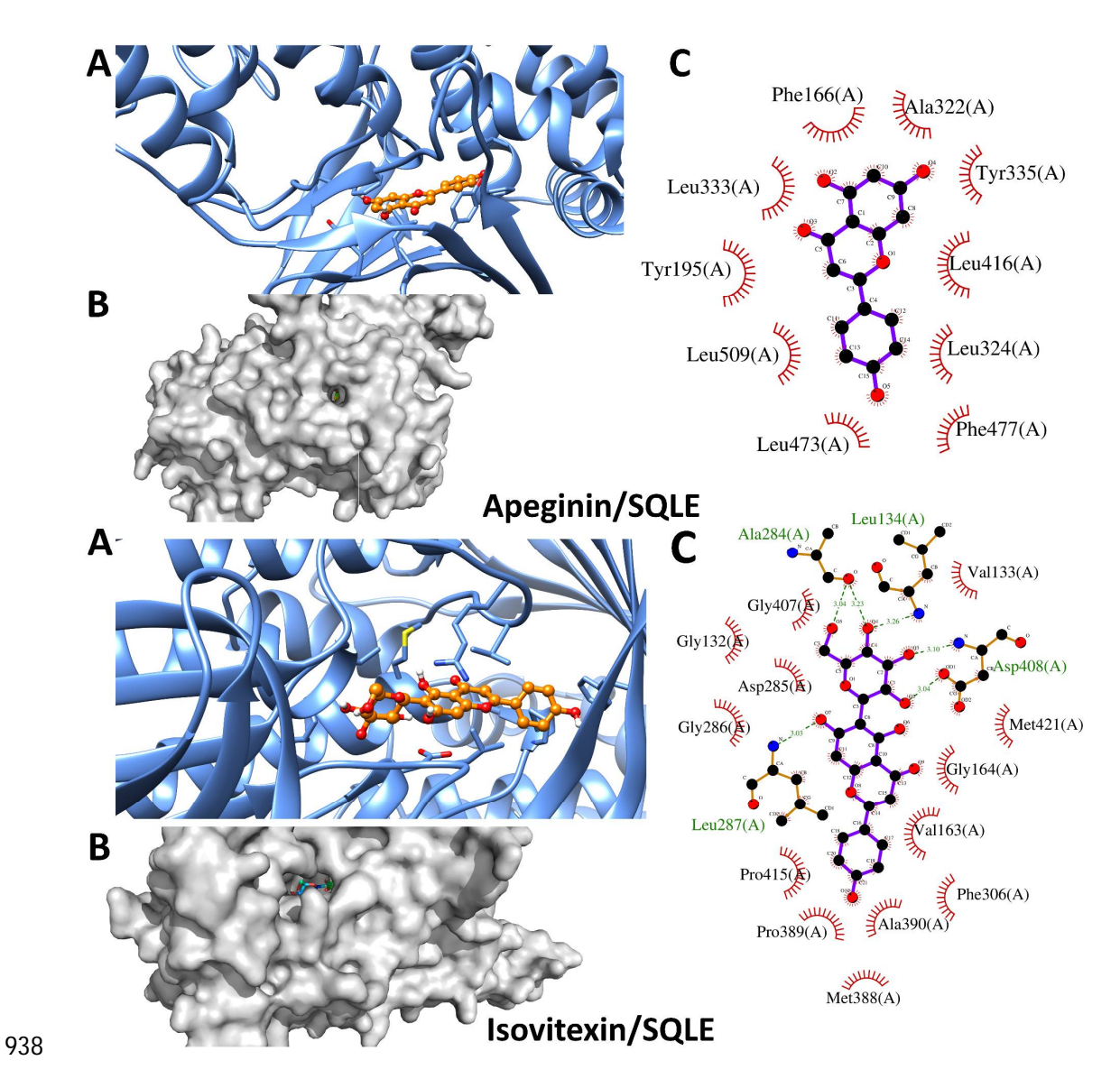


Figure 1. Docking analysis of apigenin and isovitexin against squalene epoxidase. (A) Position of the ligands within the primary binding site of squalene epoxidase, (B) Surface representation of squalene epoxidase, illustrating the ligands deeply embedded within the binding pocket, and (C) LigPlot representation highlighting polar and hydrophobic interactions between squalene epoxidase and the ligands. SQLE: squalene epoxidase.

C Tyr529(A) le528(A) Ala525(A) В Gly521(A) Phe524(A) Leu517(A) Val518(4) Neoschaftoside/SQLE C Leu287(A Met421(A) Met388(A) Gly420(Glu165(A Ile162(A) Gly164(A) (Tyr335(A) Phe166(A) Leu345(A) Vitexin/SQLE

Figure 2. Docking analysis of neoschaftoside and vitexin against squalene epoxidase. (A) Position of the ligands within squalene epoxidase, (B) Surface representation of squalene epoxidase, and (C) LigPlot representation illustrating polar and hydrophobic interactions. SQLE: squalene epoxidase.

952

947

948

949

950

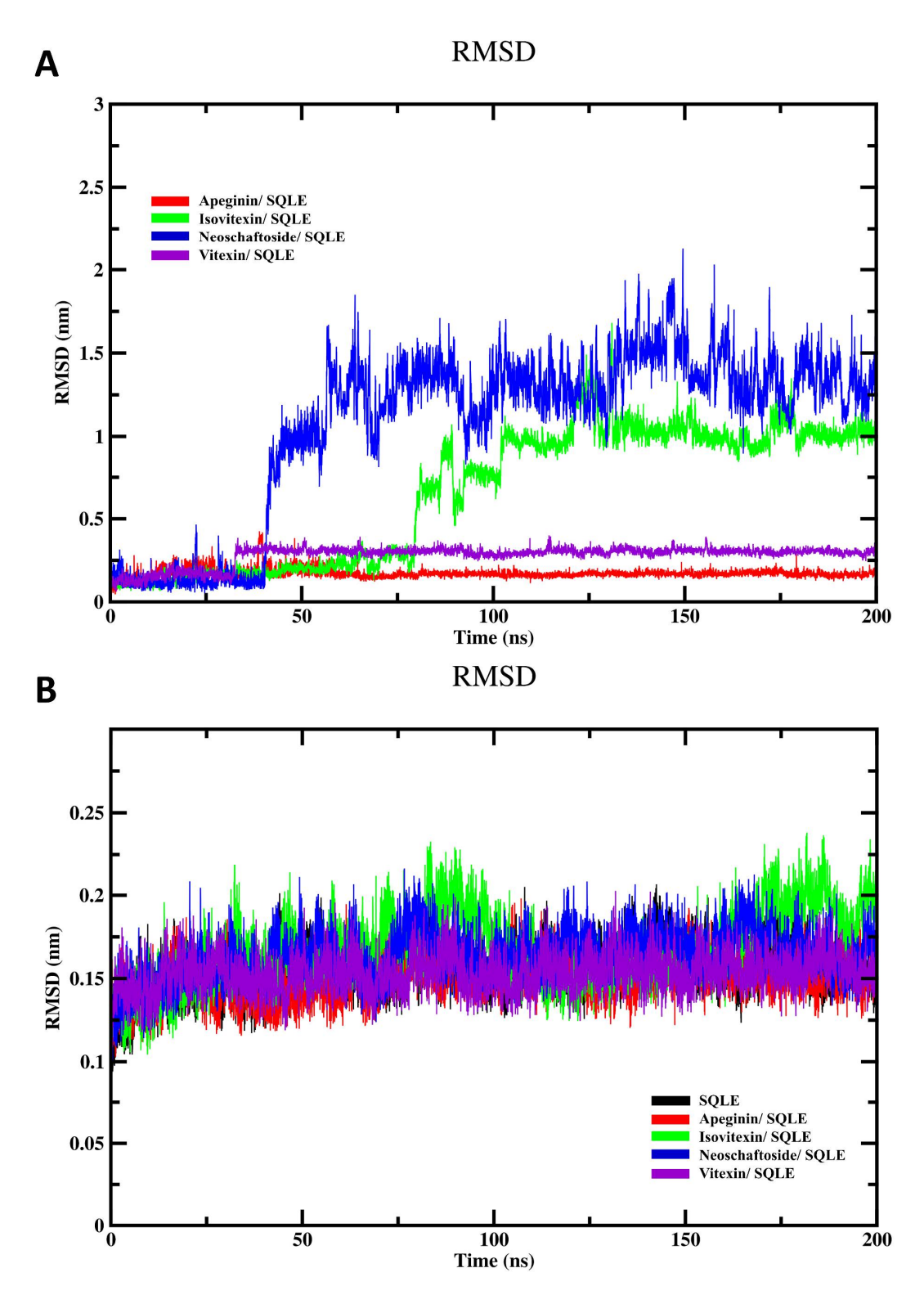


Figure 3. RMSD analysis of squalene epoxidase and its complexes with flavonoids during a 200 ns molecular dynamics simulation. (A) RMSD of the ligands relative to the

binding site of squalene epoxidase, and (B) RMSD of the enzyme backbone for the freeenzyme and its complexes with the flavonoids. SQLE: squalene epoxidase.

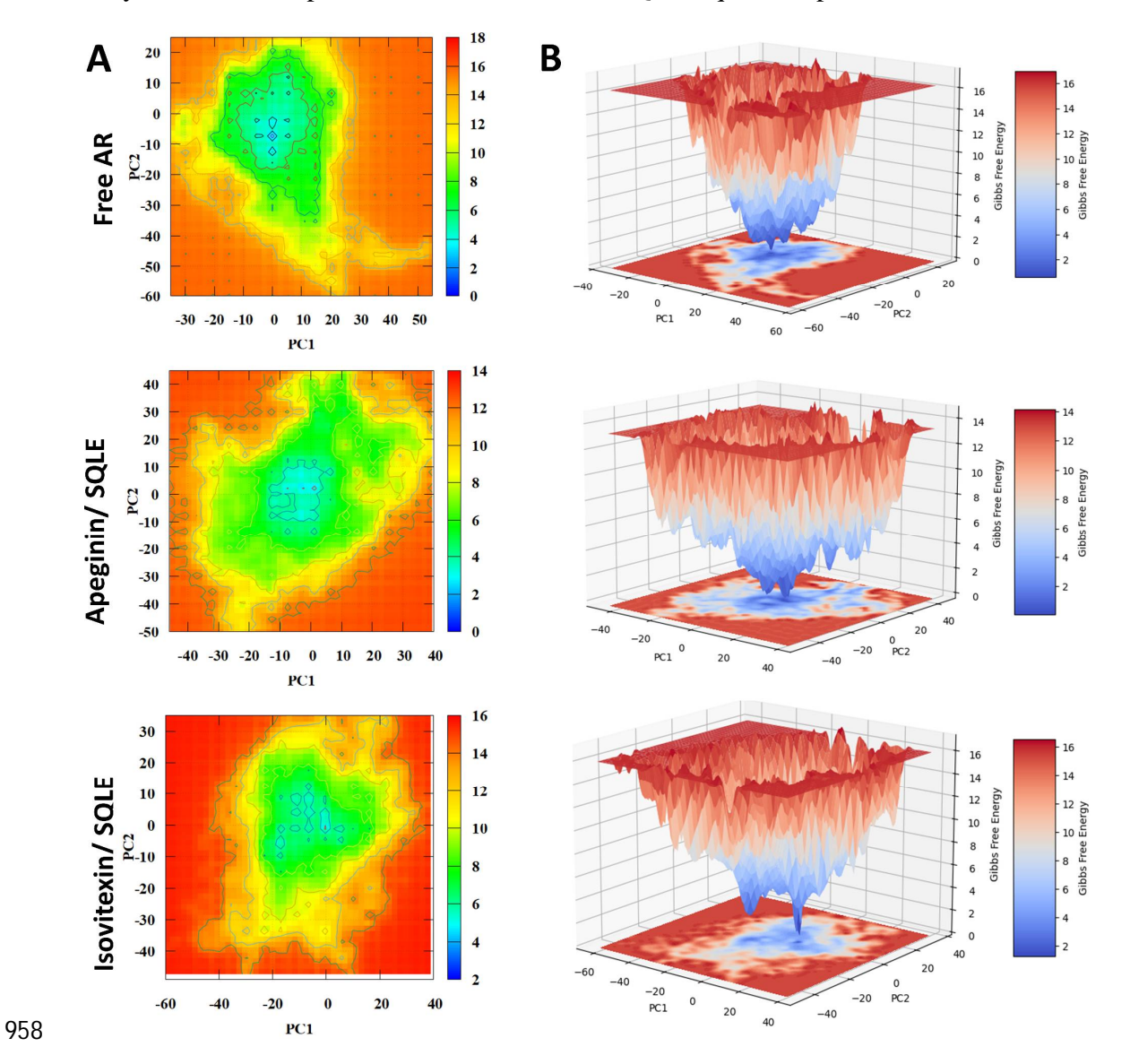


Figure 4. Potential energy landscape (PEL) of free squalene epoxidase, apigenin-bound SQLE, and isovitexin-bound squalene epoxidase. (A) 2D contour maps of the PEL constructed from principal component analysis (PCA) with PC1 and PC2 as collective variables. The color gradient represents Gibbs free energy (kcal/mol), with red indicating higher energy and blue indicating lower energy, and (B) 3D representations of the PEL.

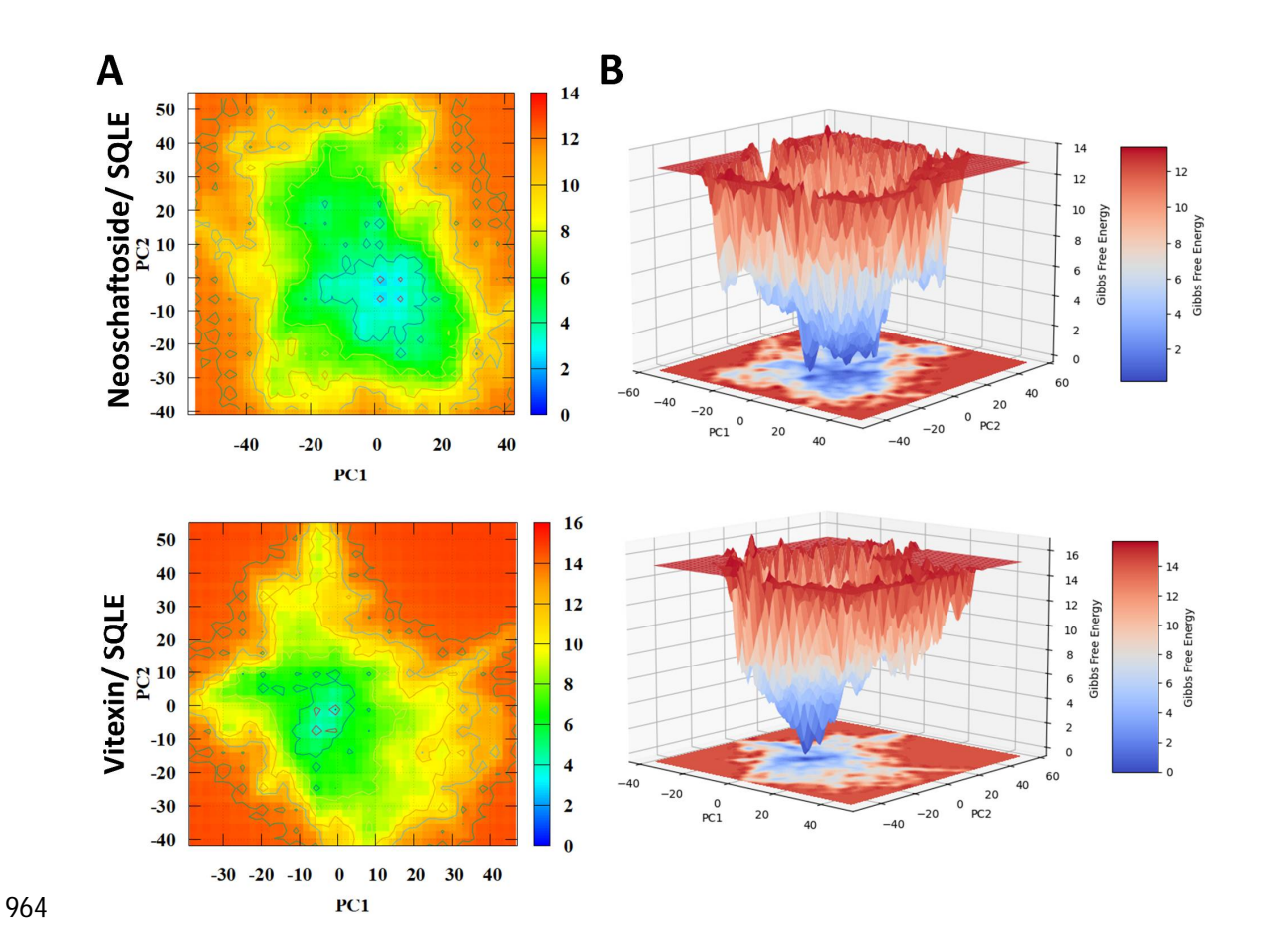


Figure 5. Potential energy landscape (PEL) of neoschaftoside- and vitexin-bound squalene epoxidase. (A) 2D contour maps of the PEL generated from PCA, with PC1 and PC2 as collective variables, and (B) 3D representations of the PEL.

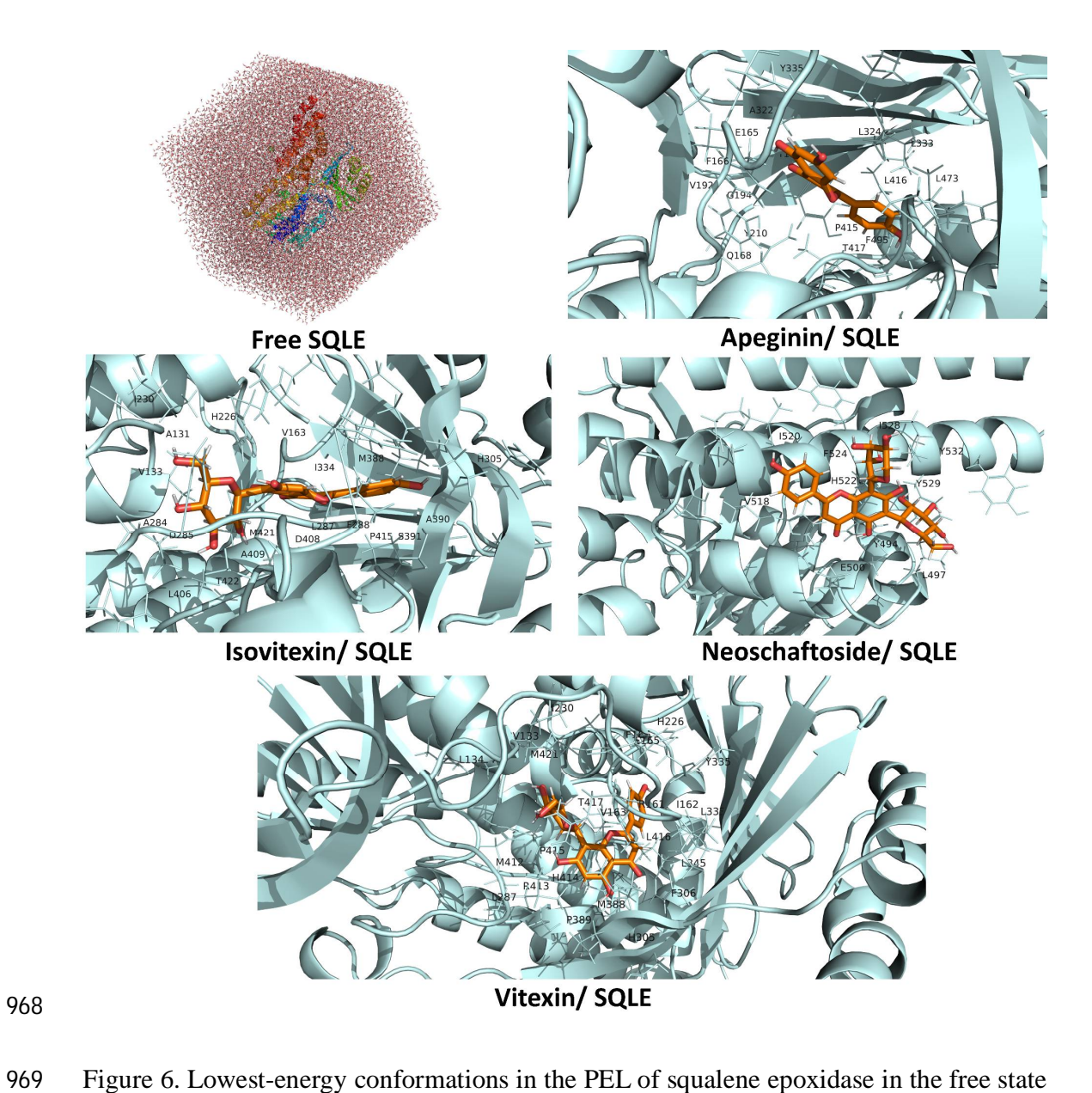


Figure 6. Lowest-energy conformations in the PEL of squalene epoxidase in the free state and in complex with flavonoids.

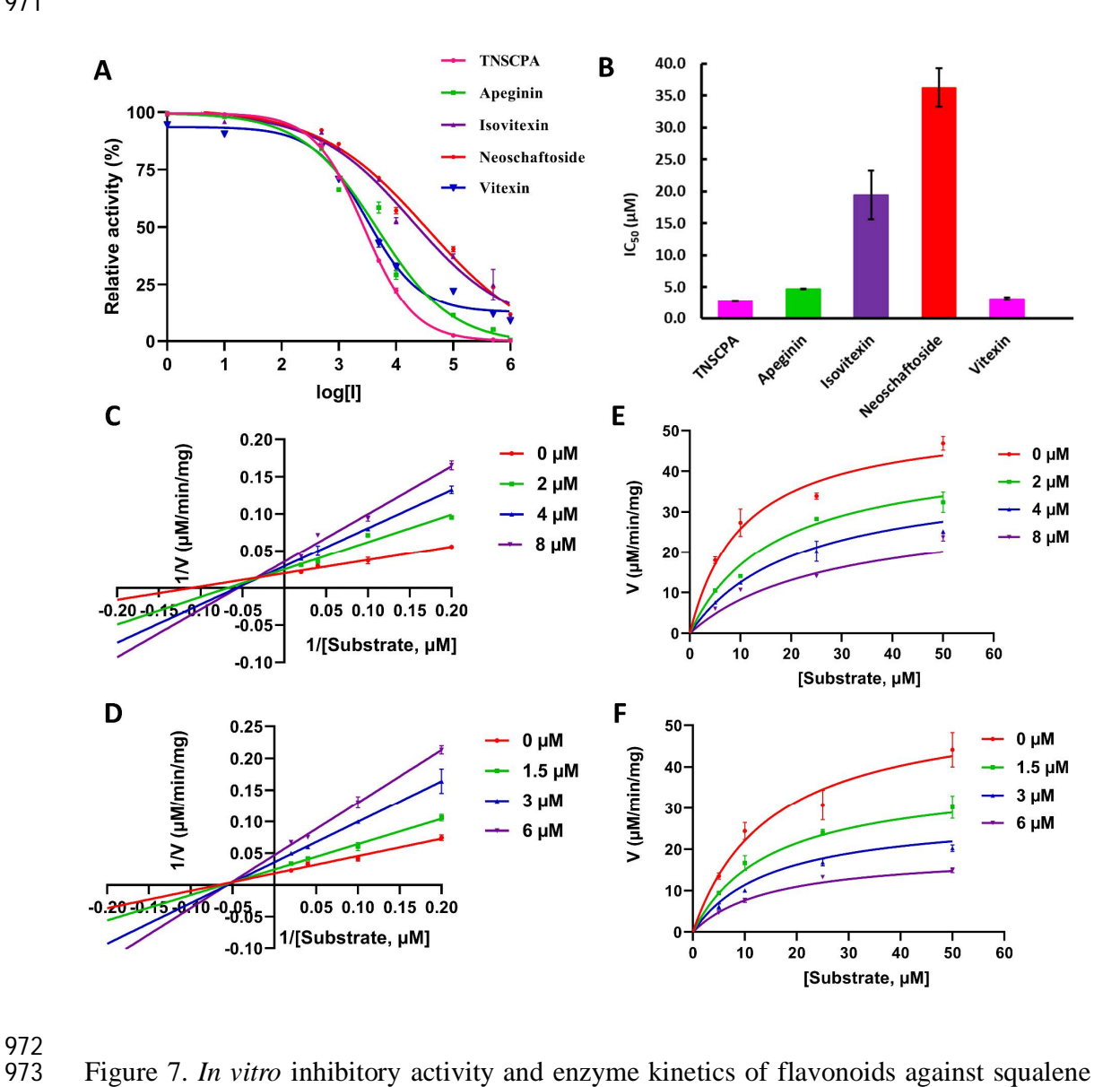


Figure 7. *In vitro* inhibitory activity and enzyme kinetics of flavonoids against squalene epoxidase. (A) Dose-response curves of the isolated flavonoids showing the percentage of relative SQLE activity at varying concentrations of each compound, (B) IC₅₀ values of the flavonoids and the reference inhibitor trisnorsqualene cyclopropylamine, calculated from the dose-response data, (C, D) Lineweaver-Burk plots for apigenin (C) and vitexin (D), and (E, F) Michaelis-Menten plots for apigenin (E) and vitexin (F). Data represent the mean ± standard deviation of three independent experiments.

Tables

Table 1: MM/PBSA computation findings for the final 50 ns of the MD trajectory (kcal/mol)

Complex	ΔE_{vdw}	ΔE_{ele}	$\Delta G_{ m solv}$	ΔG_{gas}	ΔG_{total}	
Apigenin/squalene epoxidase	-35.82 ± 0.54	-9.03 ± 1.01	21.41 ± 0.39	-44.85 ± 1.20	-23.43 ± 1.26	
Isovitexin/squalene epoxidase	-29.09 ± 0.88	-21.39 ± 3.97	34.09 ± 1.55	-34.09 ± 4.10	-16.39 ± 4.38	
Neoschaftoside/squalene epoxidase	-22.47 ± 1.17	-8.95 ± 1.38	18.52 ± 1.58	-31.42 ± 1.81	-12.90 ± 2.40	
Vitexin/squalene epoxidase	-38.59 ± 1.33	-61.29 ± 1.87	62.49 ± 1.75	-99.88 ± 2.29	-37.39 ± 2.89	
982						

Table 2. The findings of the ADMET analysis used to assess the isolated flavonoids' drug-likeness

991 characteristics.

